Myoglobin and Cytochrome b 5 : A Nuclear Magnetic Resonance Study of a Highly Dynamic Protein Complex †

ARTICLE *in* BIOCHEMISTRY · NOVEMBER 2002

Impact Factor: 3.02 · DOI: 10.1021/bi026296y · Source: PubMed

6 AUTHORS, INCLUDING:

Judith Nocek
Northwestern University
56 PUBLICATIONS **1,439** CITATIONS
SEE PROFILE

Marcellus Ubbink
Leiden University
180 PUBLICATIONS **3,572** CITATIONS
SEE PROFILE

Myoglobin and Cytochrome b_5: A Nuclear Magnetic Resonance Study of a Highly Dynamic Protein Complex†

Jonathan A. R. Worrall,‡ Yijeng Liu,§ Peter B. Crowley,‡ Judith M. Nocek,§ Brian M. Hoffman,§ and Marcellus Ubbink*,‡

Leiden Institute of Chemistry, Gorlaeus Laboratories, Leiden University, P.O. Box 9502, 2300 RA Leiden, The Netherlands, and Department of Chemistry, Northwestern University, 2145 Sheridan Road, Evanston, Illinois 60208

Received June 13, 2002; Revised Manuscript Received July 17, 2002

ABSTRACT: The transient complex of bovine myoglobin and cytochrome b_5 has been investigated using a combination of NMR chemical shift mapping, ^{15}N relaxation data, and protein docking simulations. Chemical shift perturbations observed for cytochrome b_5 amide resonances upon complex formation with either metmyoglobin (Fe^{III}) or carbon monoxide-bound myoglobin (Fe^{II}) are more than 10-fold smaller than in other transient redox protein complexes. From ^{15}N relaxation experiments, an increase in the overall correlation time of cytochrome b_5 in the presence of myoglobin is observed, confirming that complex formation is occurring. The chemical shift perturbations of proton and nitrogen amide nuclei as well as heme protons of cytochrome b_5 titrate with increasing myoglobin concentrations, also demonstrating the formation of a weak complex with a K_a in the inverse millimolar range. The perturbed residues map over a wide surface area of cytochrome b_5, with patches of residues located around the exposed heme 6-propionate as well as at the back of the protein. The nature of the affected residues is mostly negatively charged contrary to perturbed residues in other transient complexes, which are mainly hydrophobic or polar. Protein docking simulations using the NMR data as constraints show several docking geometries both close to and far away from the exposed heme propionates of myoglobin. Overall, the data support the emerging view that this complex consists of a dynamic ensemble of orientations in which each protein constantly diffuses over the surface of the other. The characteristic NMR features may serve as a structural tool for the identification of such dynamic complexes.

Transient protein complexes are formed when high turnover is required, such as in redox processes occurring in cellular metabolism. These protein complexes have a short lifetime, on the order of milliseconds. Many redox proteins show a clustering of like charged amino acids into patches on the surface. Long-range electrostatics arising from complementary charged patches on the partner proteins are perceived to assist in the formation of an initial preoriented complex. This then samples a number of orientations within the binding domain, with an optimal orientation for efficient ET[1] being achieved by short-range forces such as hydrophobic contacts and possibly H-bonds (*1*, *2*). Previously, we and others have studied a number of redox protein complexes of either physiological or nonphysiological partners using both NMR (*3*−*14*) and kinetic (*15*−*22*) methodologies. These studies have yielded the solution structures of two such transient complexes (*6*, *11*) as well as information regarding the molecular recognition sites for others (*23*, *24*).

A picture is emerging which supports the existence of two types of transient protein complexes. In the first type, the protein partners bind in a specific orientation for a significant fraction of the lifetime of the complex, utilizing both electrostatic and hydrophobic interactions (*6*, *10*, *11*, *14*, *15*), whereas in the second type, there is no specific orientation, but rather a dynamic ensemble of structures governed by electrostatics (*5*, *17*, *23*). Mb and cyt b_5 form a complex of the second type (*17*, *23*), and to further explore and understand such transient protein complexes, we have investigated the interactions between these two partners using NMR and protein docking methods.

Cyt b_5 is a low-spin heme protein responsible for ET reactions in a number of physiological processes (*25*). It exists in both membrane-bound and soluble forms. The membrane-bound form is located in the endoplasmic reticulum and the mitochondrial membrane (*26*, *27*), and consists of two domains: a hydrophilic domain (100 amino acids) and a hydrophobic domain (30 amino acids). The hydrophilic domain, which contains the *b*-type heme, is responsible for ET, while the hydrophobic domain is responsible for anchorage to the membrane. In the endoplasmic reticulum, it provides reducing equivalents for fatty acid desaturation,

† This work was supported by TMR *Haemworks* Contract FMRX-CT98-0218 and by the National Institutes of Health (Grant HL62303).

* To whom correspondence should be addressed. Phone: +31 71 527 4628. Fax: +31 71 527 4593. E-mail: m.ubbink@chem.leidenuniv.nl.

‡ Leiden University.

§ Northwestern University.

[1] Abbreviations: ET, electron transfer; cyt b_5, cytochrome b_5; met-Mb, bovine metmyoglobin; MbCO, bovine carbon monoxide-bound myoglobin; ZnMb, zinc-substituted myoglobin; met-Hb, methemoglobin; NMR, nuclear magnetic resonance; TSP, sodium 3-(trimethylsilyl)-d_4-propionate; HSQC, heteronuclear single-quantum coherence; CPMG, Carr−Purcell−Meiboom−Gill; T_1, longitudinal relaxation time; T_2, transverse relaxation time; BiGGER, biomolecular complex generation with global evaluation and ranking.

10.1021/bi026296y CCC: $22.00
Published on Web 09/07/2002

cholesterol biosynthesis, and the oxidation of certain substrates by cytochrome P450s (*28*, *29*). Trypsin proteolysis of membrane-bound cyt b_5 produces the soluble N-terminal fragment, consisting of 84 residues, of which an X-ray crystal structure has been determined (*30*).

It has been suggested that a further function for cyt b_5 is in a repair process, where a soluble form reduces met-Hb and met-Mb, neither of which in the Fe(III) state can bind oxygen (*31*, *32*). Transient absorption kinetic experiments with cyt b_5 and Mb from sperm whale and horse species indicated that both Mbs form weak complexes with cyt b_5 (*17*, *33*). Kinetic, ^{1}H NMR, and isothermal calorimetry studies (*34*) recently revised an earlier ^{1}H NMR study of the Mb−cyt b_5 complex, which reported a large association constant (*32*). Kinetic studies of the complex with wild-type (wt) Mb and with Mb in which the heme propionates had been neutralized, in parallel with Brownian dynamics and ET pathway calculations, led to the development of a new "dynamic docking" model for highly dynamic protein−protein complexes (*23*). This model postulates that cyt b_5 binds to a large area on the Mb surface, in a wide variety of conformations. There is no specific or favored orientation for this unstable complex, but only a small subset of its many conformations are ET-active; these have cyt b_5 bound in the vicinity of the heme edge. The subset of conformations that dominates the ET rate constant is not the most favorable for binding and does not contribute significantly to the thermodynamic binding constant. Such decoupling is clearly of physiological relevance for the reduction of met-Mb in muscle and of met-Hb in red cells, where tight binding of cyt b_5 to the high concentration of ferrous-Mb/Hb would prevent the cytochrome from finding and reducing the oxidized proteins.

The possibility of isotopically labeling a cyt b_5 identical to the trypsin-solubilized form of bovine liver cyt b_5 (residues 3−84), through the availability of an expression system in *Escherichia coli* (*35*), allows the use of heteronuclear NMR in testing this picture of the interaction of cyt b_5 with bovine Mb. Both met-Mb (Fe^{III}) and MbCO (Fe^{II}) were used to study the interaction, as evidence from previous studies of transient complexes has indicated that the active site charge at one or both of the partners can cause differences in complex formation (*10*, *36*, *37*). The combined use of NMR chemical shift mapping, ^{15}N relaxation experiments, and the protein docking program BiGGER (*38*) provides structural evidence that the proteins indeed undergo dynamic docking whereby they form a weak affinity complex with a dynamic ensemble of orientations.

MATERIALS AND METHODS

Protein Isolation. Oxymyoglobin was isolated from a single bovine heart according to published procedures (*39*, *40*). The gene for the trypsin-solubilized fragment of bovine cytochrome b_5 was overexpressed in *E. coli* using the expression system of Funk et al. (*35*). A single colony obtained from a transformation plate was used to inoculate 30 mL of Bio-Express 1000 medium (∼96% ^{15}N enrichment, Cambridge Isotopes Laboratories). Protein expression was activated after 5 h, by adding IPTG, and the culture was further incubated overnight. Next, a 10 mL aliquot of this culture was used to inoculate 1 L of M9 minimal medium containing $(^{15}NH_4)_2SO_4$ (Martek), supplemented with an additional 15 mL of Bio-Express 1000 medium, $CaCl_2$, $MgSO_4$, ferric citrate, glycerol, and ampicillin. After overnight incubation, cells were harvested by centrifugation at 10000*g* (Sorvall). The protocol described by Reid and Mauk for isolating the native hepatic protein from microsomes (*41*) was adapted to isolate protein from the bacterial cells. From 1 L of medium, 20−30 mg of cyt b_5 was obtained.

Preparation of NMR Samples. Oxidized cyt b_5 and met-Mb were prepared by addition of an excess (2−3-fold) of $K_3[Fe(CN)_6]$ followed by dialysis under nitrogen against 10 mM potassium phosphate (pH 6.0) by ultrafiltration methods (Amicon, YM3 membrane). MbCO was prepared by reduction of met-Mb with a slight excess of sodium dithionite followed by subsequent flushing of the sample with CO. Protein concentrations for oxidized cyt b_5 were determined spectrophotometrically according to the absorbance peak at 414 nm ($\epsilon = 117$ mM^{-1} cm^{-1}) (*42*). For met-Mb and MbCO, the absorbance maxima at 408 nm ($\epsilon = 188$ mM^{-1} cm^{-1}) and 424 nm ($\epsilon = 207$ mM^{-1} cm^{-1}), respectively, were used (*39*).

NMR samples of ^{15}N-labeled cyt b_5 (0.5−5.4 mM) were prepared in 10 mM potassium phosphate buffer (pH 6.0) and contained 6% D_2O for lock, as well as 100 μM TSP and [^{15}N]acetamide ($CH_3CO^{15}NH_2$) as internal references. For met-Mb and MbCO, NMR samples were prepared in an identical manner to give final protein concentrations ranging from 1.7 to 2.5 mM. The pH for all protein samples was adjusted to pH 6.00 ± 0.05, and the solutions were degassed with argon.

NMR Titration Experiments. All NMR experiments were performed at 14.1 T on a Bruker DMX600 spectrometer operating at 300 K equipped with a TXI-Z-GRAD (^{1}H, ^{13}C, and ^{15}N) probe. For the titration experiments, spectra were first recorded with free ^{15}N-labeled ferric cyt b_5, followed by titration of either met-Mb or MbCO into the initial sample. For the titration with met-Mb, an initial ferric cyt b_5 concentration of 0.75 mM was used with a final molar ratio of 1:2.5 (cyt b_5:met-Mb), while for the MbCO titration, an initial ferric cyt b_5 concentration of 0.54 mM was used with a final molar ratio of 1:2.0 (cyt b_5:MbCO). A reverse titration was also performed with ^{15}N-labeled ferric cyt b_5 titrated into either met-Mb or MbCO to give a final molar ratio in both cases of 1:1. Before and after each titration step, the pH of the sample was verified. As a control experiment, a pH titration was performed on ferric cyt b_5, in the pH range of 6.2−5.8. This further confirmed that the cross-peaks affected upon interaction with Mb were due to complex formation and not to pH effects. All titration experiments were recorded using one-dimensional (1D) proton and two-dimensional (2D) ^{15}N,^{1}H-HSQC (*43*) spectra. Spectral widths in kilohertz of 48 for proton 1D and 2.4 (^{15}N, F_1) and 11 (^{1}H, F_2) for 2D ^{15}N,^{1}H-HSQC spectra were employed. Data processing of the 1D proton spectra was performed in XWINNMR, and the ^{15}N,^{1}H-HSQC spectra were processed in AZARA (available from ftp://ftp.bio.cam.ac.uk/pub/azara). Assignments of the ^{15}N and ^{1}H nuclei of ferric cyt b_5 were aided by known literature assignments (*9*, *44*). Amides which were unassigned in the current work were A3, S18, S20, F35, G41, G42, L70, and I76. Chemical shift perturbations of ^{15}N and ^{1}H nuclei for cyt b_5 upon interaction with Mb were analyzed by overlaying the spectra of bound cyt b_5 with those of the free protein in the assignment program ANSIG (*45*, *46*). The

average amide chemical shift perturbation ($\Delta\delta_{avg}$) was calculated by using eq 1

$$\Delta\delta_{avg} = \sqrt{\frac{(\Delta\delta N/5)^2 + \Delta\delta H^2}{2}} \quad (1)$$

in which $\Delta\delta$N represents the change in the amide nitrogen's chemical shift and $\Delta\delta$H represents the change in the amide proton's chemical shift (*47*).

NMR Relaxation Experiments. ^{15}N longitudinal (T_1) and transverse (T_2) relaxation rates at 300 K were measured at 14.1 T, corresponding to a ^{15}N Larmor frequency of 60.8 MHz. Experiments were performed first on free ferric [^{15}N]-cyt b_5 (56 mg/mL, pH 6.0) followed by cyt b_5 in a 1:1 stoichiometry with met-Mb (total protein concentration of 56 mg/mL, pH 6.0). Three-dimensional (3D) versions of ^{15}N,^{1}H-HSQC experiments were implemented using the pulse sequences described by Kay et al. (*48*), in an interleaved fashion with a ^{1}H(t_2)−VD−^{15}N(t_1) acquisition order, where VD is the variable delay time for the relaxation delay. For both ^{15}N T_1 and T_2 experiments, 204 complex t_1 increments and 2K t_2 points with 16 scans per t_1 point were employed, with spectral widths of 1.9 kHz (^{15}N F_1) and 9 kHz (^{1}H F_3). In the T_1 experiment for free ferric cyt b_5, 10 different variable delay times (10, 18, 32, 60, 110, 180*, 320, 500, 640, and 900 ms) were used to obtain the ^{15}N T_1 relaxation times. For cyt b_5 in complex with met-Mb, values for the longitudinal relaxation period of 10, 100, 180*, 260, 350, 440, 550, 640, 900, and 1200 ms were employed. Asterisks indicate points acquired in duplicate. The relaxation delay between scans was 2.5 s. In the T_2 experiments, for both the free and bound cyt b_5, 10 different variable delay times for the duration of the CPMG sequence (0, 18, 36*, 54, 72, 108, 144, 180, 216, and 252 ms) were employed to obtain the ^{15}N T_2 relaxation rates. The delay between 180° pulses in the CPMG sequence was set to 1 ms, and a recycle delay of 2.5 s was used between scans. All data processing was performed in AZARA to yield a final ^{15}N, ^{1}H point matrix of 256 × 2048 real data points in Fourier-transformed spectra.

Analysis of ^{15}N Relaxation Rates and Estimation of the Global Correlation Time. ^{15}N T_1 and T_2 relaxation rates were obtained by fitting the peak intensities as a function of the relaxation delay to a single-exponential decay by using the Levenberg−Marquardt algorithm (*49*). The standard errors in the fitted parameters were determined from the scatter of the data points around the exponential curve, and from the duplicate relaxation delays in the variable delay lists. They ranged from 0.2 to 8% for T_1 and were between 0.1 and 7% for the T_2 fitting of the free protein. For a 1:1 stoichiometry with met-Mb, they ranged from 0.1 to 5% for T_1 and from 0.3 to 6% for T_2.

The overall rotational correlation time (τ_r) was estimated from a trimmed mean value of the T_1/T_2 (R_2/R_1) ratio by solving the equation (*50*)

$$\frac{R_2}{R_1} = \{4J(0) + J(\omega_N - \omega_H) + 3J(\omega_N) + 6J(\omega_N + \omega_H) + (c^2/3d^2)[4J(0) + 3J(\omega_N)]\}/[2J(\omega_N - \omega_H) + 6J(\omega_N) + 12J(\omega_N + \omega_H) + 2(c^2/3d^2)J(\omega_N)] \quad (2a)$$

in which

$$J(\omega) = \frac{2}{5}S^2\left[\frac{\tau_r}{1 + (\omega\tau_r)^2}\right] \quad (2b)$$

where τ_r is the correlation time for the overall tumbling of the molecule and S^2 is the generalized order parameter characterizing the amplitude of internal motions (note that the factor $^2/_5S^2$ drops out of eq 2). In eq 2a, $c = \mu_o h\gamma_N\gamma_H(r_{NH}^{-3})/(8\pi)^2$ and $d = \omega\Delta\sigma/\sqrt{3}$, where μ_o is the permeability of free space, h is Planck's constant, γ_N and γ_H are the gyromagnetic ratios of the ^{1}H and the ^{15}N spin, respectively, r_{NH} is the N−H bond length (1.04 Å), ω_H and ω_N are the Larmor frequencies of ^{1}H and ^{15}N spins, respectively, in radians per second, and $\Delta\sigma$ is the chemical shift anisotropy (−160 ppm) of the ^{15}N spin (*50*). Equation 2 only holds for residues that experience very fast internal motions (*51*, *52*). Residues that experience slower motions or exchange will demonstrate deviating T_1/T_2 ratios. Therefore, all residues with T_1/T_2 ratios that differed by more than 10% from the mean were excluded from the calculations of the overall correlation time.

Protein Docking. The coordinates for horse met-Mb (*53*) and cyt b_5 (*30*) were taken from the Protein Data Bank (entries 1HMB and 1EHB, respectively). Using the docking program BiGGER (available from http://www.dq.fct.unl.pt/bioin/chemera/), docking simulations between horse met-Mb and cyt b_5 were performed. The program consists of two modules (*38*), with the first generating a population of docked geometries with maximal surface matching and favorable intermolecular amino acid contacts. This is achieved by representing the shape of each molecule with a 3D matrix of 1 Å^3 cells and then using this matrix for an exhaustive grid search in which the matrix defining one molecule systematically explores the matrix representing the partner molecule. In the second module, the docking results were ranked either according to a global scoring function, composed of four terms, surface matching, side chain contacts, electrostatics, and solvation energy or according to NMR data. In the latter case, cyt b_5 amides which experienced an $\Delta\delta_{avg}$ of ≥0.005 ppm were translated into distance constraints on the assumption that they must be within 5 Å of any atom (atom surface−atom surface distance) on met-Mb. The scoring is based on the number of satisfied constraints in each of the docked geometries.

RESULTS

1D NMR Titrations of Met-Mb and MbCO to Ferric Cyt b_5. Because of the paramagnetic properties of low-spin ferric cyt b_5 ($S = {}^1/_2$), a number of well-resolved signals are observed downfield (12−30 ppm) in the 1D proton NMR spectra. These signals arise from proton nuclei of the heme which experience a Fermi contact interaction with the unpaired electron residing on the iron atom (*54*, *55*). In addition, a number of less intense signals are observed in the same region due to a minor form of cyt b_5, in which the heme is inserted into the protein rotated by 180° around the α−γ meso carbon axis relative to the major form (*56*, *57*). Assignments of these signals for both major and minor isoforms have previously been reported (*58*).

On addition of microliter aliquots of met-Mb or MbCO to ferric cyt b_5, a number of these downfield-shifted signals

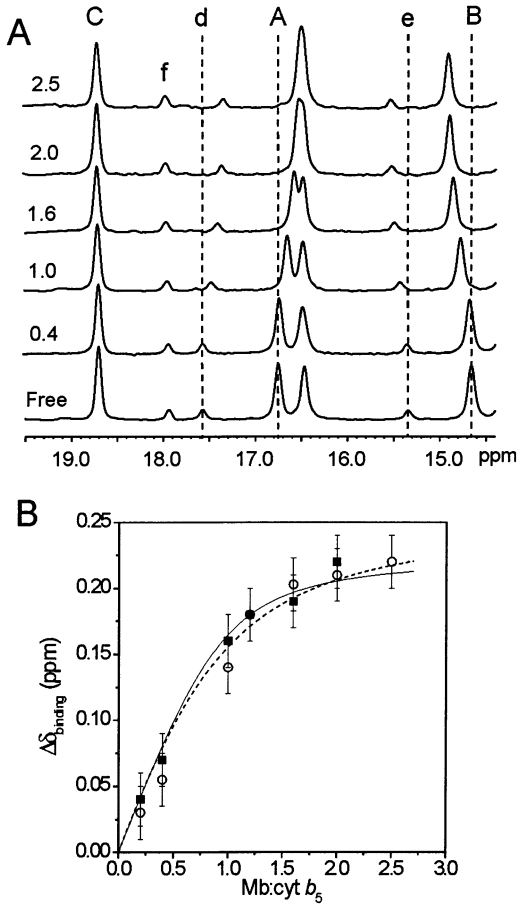

FIGURE 1: 1D ^{1}H NMR data for the titration of Mb into ferric cyt b_5 (10 mM potassium phosphate, pH 6.0, 300 K). (A) Downfield hyperfine-shifted signals of ferric cyt b_5 in the absence (Free) and with an increasing ratio of met-Mb. Peaks A and B are assigned to the 6-α-propionate methylene protons for the major form, and peaks d and e correspond to the 7-α-propionate methylene protons of the minor form. The dashed lines guide the eye for the titrating peaks. Peak C is 7-α-propionate methylene of the major form and peak f the 4-α-vinyl of the minor form which do not titrate with increasing amounts of Mb. (B) Titration curves for peak B of ferric cyt b_5 with increasing amounts of met-Mb (○) and MbCO (■). Chemical shift changes ($\Delta\delta_{binding}$) are plotted as a function of the Mb over the cyt b_5 ratio and fit assuming a 1:1 complex, with K_as of 5 and 20 mM^{-1} for the met-Mb (- - -) and MbCO (—) titrations, respectively.

are perturbed. These signals are assigned to the 5-methyl and 6-α-propionate methylene protons in the major from and the 8-methyl and 7-α-propionate methylene protons in the minor from (Figure 1A). The gradual change in chemical shift of these signals during the titration is indicative of a fast exchange process on the NMR time scale ($k_{ex} \gg 500$ s^{-1}), resulting in a single averaged resonance for the perturbed peak of cyt b_5 upon interaction with Mb. The chemical shift changes ($\Delta\delta_{binding}$) can be fitted to a 1:1 binding model (*5*), yielding binding constants, K_a, of 5(3) and 20(5) mM^{-1} for the met-Mb and MbCO titrations, respectively (Figure 1B). The former is in satisfactory agreement with recent ^{1}H NMR and isothermal calorimetry measurements (*34*).

Inspection of the crystal structure of cyt b_5 (*30*) indicates that the 6-propionate in the major form extends out of the heme pocket and into the solvent. Similarly, it is most likely that in the minor form the 7-propionate extrudes from the protein. These observations strongly suggest that the chemical shift perturbations observed in both the major and minor isoforms for the propionate methylene protons on addition of Mb arise due to a change in the chemical environment caused by binding configurations with close contact between the Mb surface and the heme region of cyt b_5.

2D NMR Titrations of Met-Mb and MbCO to Cyt b_5. To further analyze this protein−protein interaction by NMR, a series of 2D ^{15}N,^{1}H-HSQC spectra of ^{15}N-labeled ferric cyt b_5 were recorded in the presence of increasing amounts of either met-Mb or MbCO. In both titrations, small $\Delta\delta_{binding}$ values for a number of ^{15}N and ^{1}H nuclei of ferric cyt b_5 were observed ($\geq$0.01 for ^{1}H and $\geq$0.05 ppm for ^{15}N), suggesting that these residues are affected during interaction with Mb. The appearance of a single averaged resonance for the perturbed cross-peak is again consistent with a fast exchange process on the NMR time scale (Figure 2A,B).

For the significantly perturbed cross-peaks, titration curves were plotted, and fit to a 1:1 binding model (Figure 2C). The fits are consistent with the 1D data with K_as of 5(3) and 20(5) mM^{-1} being obtained for the met-Mb and MbCO titrations, respectively. It would thus appear that the cyt b_5−MbCO interaction is slightly stronger.

This difference is surprising when it is considered that the loss of a +1 charge at the Mb heme should conceivably lead to a weaker binding interaction, and it should be noted that a determination of K_a by NMR methodology is not the most accurate, especially when the $\Delta\delta_{binding}$ is small (<0.03 ppm for H^N). However, for all significantly perturbed resonances in the 2D spectra, titration curves can be plotted and fitted to give an acceptable K_a in agreement with reported values (*33*, *34*). To exclude the possibility that the small shifts were caused by changes in pH, a pH titration was performed in the pH range of 6.2−5.8 for ferric cyt b_5. It demonstrated that none of the resonances that are perturbed by addition of Mb are significantly affected by pH. Additionally, in a reverse titration, of ferric cyt b_5 to met-Mb and MbCO, the same resonances were affected as in the normal titration. It is therefore concluded from the 1D and 2D titration experiments that the perturbed resonances for cyt b_5 on addition of Mb are caused by complex formation. This is further supported by the ^{15}N relaxation data (vide infra).

Chemical Shift Mapping of the Interaction Domain on Ferric Cyt b_5. In Figure 3, the $\Delta\delta_{avg}$ amide chemical shifts are plotted as a function of cyt b_5 residue number in the presence of 2.5 molar equiv of met-Mb and 2.0 molar equiv of MbCO. For both titrations, a total of 15 significant $\Delta\delta_{avg}$ amide chemical shifts are observed for cyt b_5. With the exceptions of R84 in the met-Mb titration and A54 in the MbCO titration, the same amides are affected for both titrations (Table S1). In Figure 4, the $\Delta\delta_{avg}$ amide chemical shifts for ferric cyt b_5 upon interaction with met-Mb and MbCO have been color-coded according to the size of their $\Delta\delta_{avg}$ and mapped onto the surface of the protein. The majority of the affected residues map onto the front face surrounding the highly exposed heme 6-propionate, for which a $\Delta\delta_{binding}$ was observed in the 1D experiments. Two negatively charged patches (E43, E44, and E48 and E56, E59, and D60) on either side of the heme would appear to be primarily involved in complex formation, with additional effects seen for one of the coordinating histidines (H63) and residues in the proximity (V61, G62, and S64). From

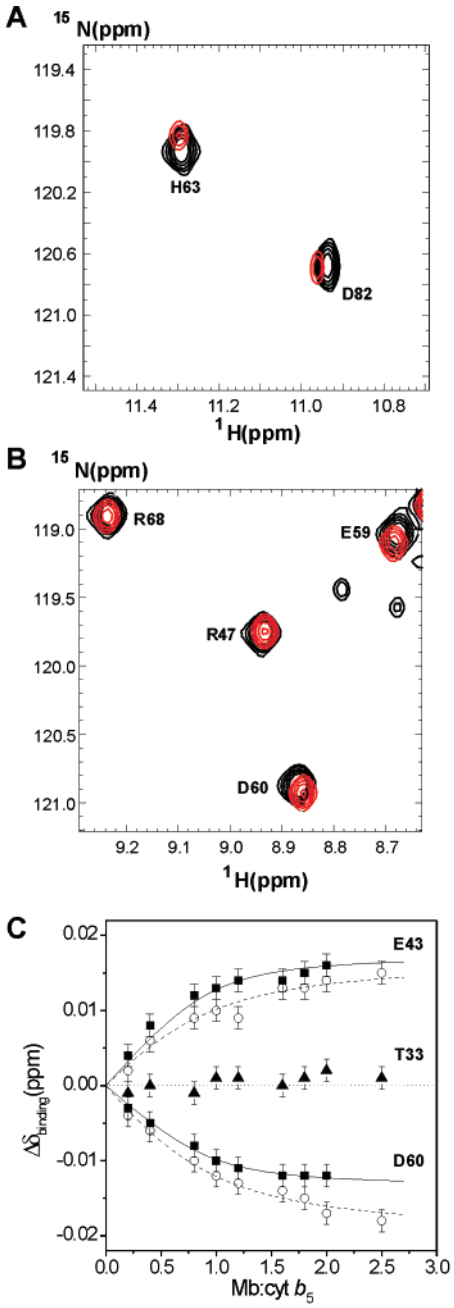

FIGURE 2: 2D NMR data for the titration of Mb into ferric cyt b_5 (10 mM potassium phosphate, pH 6.0, 300 K). Overlay of part of the ^{15}N,^{1}H-HSQC spectra of ferric cyt b_5 in the free form (black) and with 2.5 equiv of met-Mb (red) (A) and 2.0 equiv of MbCO (red) (B). (C) Titration curves for the $\Delta\delta_{binding}$ for the H^N of E43 and D60 of ferric cyt b_5 with increasing amounts of met-Mb (○) and MbCO (■). Curves are fitted assuming a 1:1 complex, with K_as of 5 and 20 mM^{-1} for the met-Mb (- - -) and MbCO (—) titrations, respectively. Triangles indicate the change in H^N chemical shift for a nonaffected residue (T33) in the complex.

Table 1: Average T_1 and T_2 Values (seconds), T_1/T_2 Ratios, and Trimmed $*T_1/T_2$ Ratios for Backbone Amide ^{15}N Nuclei of Free Ferric Cyt b_5 and for Cyt b_5 in a 1:1 Stoichiometry with Met-Mb at 600 MHz (10 mM potassium phosphate, pH 6.0, 300 K)[a]

	free ferric cyt b_5	cyt b_5 in a 1:1 stoichiometry with MetMb
T_1	0.59 (0.03)	0.67 (0.03)
T_2	0.10 (0.01)	0.077 (0.006)
T_1/T_2	5.9 (0.9)	8.7 (1.1)
$*T_1/T_2$	5.8 (0.3)	8.6 (0.5)
T_1 for Trp22 $N^{\epsilon 1}$	0.45 ± 0.04	0.78 ± 0.01
T_2 for Trp22 $N^{\epsilon 1}$	0.14 ± 0.003	0.10 ± 0.001

[a] The numbers in parentheses indicate the standard deviation. Relaxation parameters (seconds) for Trp22 $N^{\epsilon 1}$ are also included.

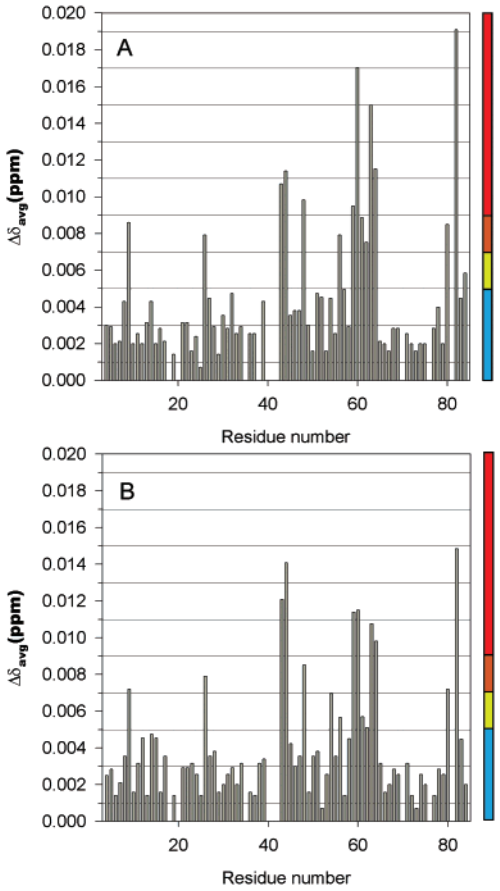

FIGURE 3: Changes in the chemical shifts of cyt b_5 residues on titration with met-Mb and MbCO. The changes in average amide chemical shift ($\Delta\delta_{avg}$) of cyt b_5 upon (A) titration with met-Mb (1:2.5 molar ratio) and (B) titration with MbCO (1:2.0 molar ratio) are plotted as a function of cyt b_5 residue number. The vertical color strips categorize the changes in $\Delta\delta_{avg}$ into high (red), medium (orange), low (yellow), and not significant (blue) for mapping onto the three-dimensional structure of cyt b_5 in Figure 4.

structural studies on a V61H cyt b_5 mutant, it is shown that the loop containing Phe58−Gly62 is sensitive to structural perturbations in this region of the protein (*30*). It would appear that this is also the case when a redox partner binds. In addition, surface residues located away from this recognition site are also perturbed upon interaction with both forms of Mb. These residues consist of L9, H80, D82, and R84 (met-Mb only) and are located in the N- and C-terminal regions of the protein (Figure 4). These residues are too far away from the "front" face of the protein to be affected by secondary chemical shift changes as previously seen for other transient complexes (*5*, *10*), and thus must be involved in a different binding orientation in keeping with the dynamic binding model.

^{15}N Relaxation Data for Free Ferric Cyt b_5 and in Complex with Met-Mb. To further characterize formation of the complex between Mb and cyt b_5, ^{15}N T_1 and T_2 measurements were performed on cyt b_5, both free and in a 1:1 stoichiometry with met-Mb. The T_1/T_2 ratio allows an estimate of the overall correlation time (τ_r) to be determined, which should

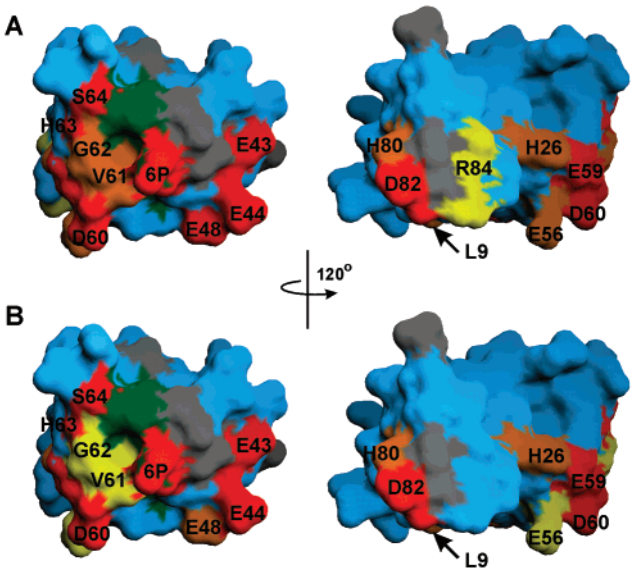

FIGURE 4: Surface representations of cyt b_5 that experience amide chemical shift changes on binding (A) met-Mb and (B) MbCO [drawn using GRASP version 1.3 (*59*)]. Size categories of $\Delta\delta_{avg}$ for amides are indicated by the vertical color strips in Figure 3 (red > orange > yellow), with blue representing unaffected residues, gray unassigned or proline residues, and green the exposed heme. Residues are identified with the single-letter amino acid code, and 6P represents the heme 6-propionate. The surfaces on the right have been rotated 120° around the vertical axis, with respect to those on the left.

be substantially increased when the 9 kDa cyt b_5 forms a complex with the 18 kDa Mb.

Of the 73 assigned backbone amides for cyt b_5, 70 were sufficiently resolved to obtain ^{15}N T_1 and T_2 values. The fact that the ferric form of cyt b_5 is paramagnetic must also be considered. For a low-spin Fe^{III} species, the effect of paramagnetism on proton relaxation is expected to be non-negligible, whereas the effect is much less pronounced for the ^{15}N nucleus, due to its lower gyromagnetic ratio with respect to the ^{1}H nucleus (*60*). On the basis of previous ^{15}N relaxation studies with paramagnetic proteins, ^{15}N nuclei within 7 Å of the paramagnetic center should be omitted (*61*, *62*). For cyt b_5, the backbone amides of Gly42 (5.1 Å) and His63 (7 Å) were thus removed, to yield a final data set of 68 backbone amides for which T_1 and T_2 relaxation rates could be obtained for both free cyt b_5 and in complex with met-Mb. Values for individual amide T_1 and T_2 times and the T_1/T_2 ratio for both free and bound cyt b_5 are given in Table S2.

The average T_1 and T_2 times for free cyt b_5 and the T_1/T_2 ratio are given in Table 1, with individual amide values plotted versus residue number in Figure 5. These are in agreement with previously published values on a non-trypsin-solubilized form of bovine cyt b_5 (104 amino acids), if different conditions and field strengths are taken into account (*63*). It is noted from Figure 5 that Tyr27 has a significantly higher T_1/T_2 ratio, resulting from a shorter T_2 rate. This suggests that the amide group of Tyr27 experiences a chemical exchange process or a conformational equilibrium on the micro- to millisecond time scale (*64*). In general, however, from the uniform relaxation rates it would appear that on the sub-nanosecond time scale the backbone of cyt b_5 is relatively rigid. Apart from the backbone nitrogens, cyt b_5 harbors a side chain nitrogen on a tryptophan residue,

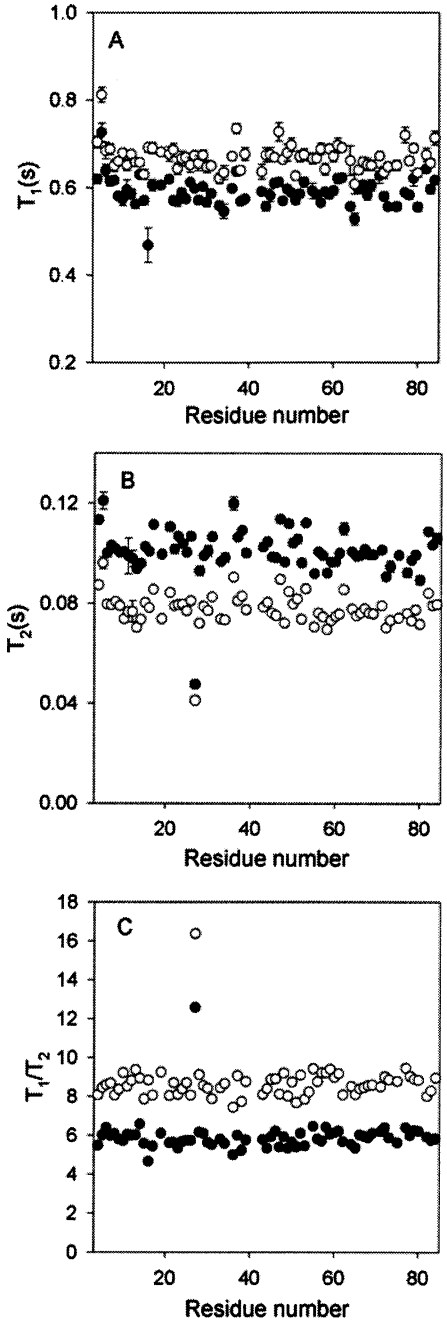

FIGURE 5: ^{15}N relaxation data for free cyt b_5 (●) and for cyt b_5 in a 1:1 stoichiometry with met-Mb (○) at 600 MHz (10 mM potassium phosphate, pH 6.0, 300 K). The observed relaxation data for the individual amides are plotted vs residue number for (A) ^{15}N T_1, (B) ^{15}N T_2, and (C) the T_1/T_2 ratio.

Trp22. The relaxation data for the $N^{\epsilon 1}$ are also summarized in Table 1.

Maintaining conditions similar to those of the free protein is important if a comparison between the bound and free protein is to be made, as the relaxation rates can be influenced by different sample conditions such as viscosity. Therefore, relaxation rates were measured for cyt b_5 in a 1:1 stoichiometry with met-Mb in a solution with the same total protein weight per volume (56 mg/mL) in the sample. The average T_1 and T_2 times increase and decrease, respectively; thus, the T_1/T_2 ratio increases (Table 1 and Figure 5). This is as expected when complex formation increases the molecular mass of the sample, leading to an increase in the

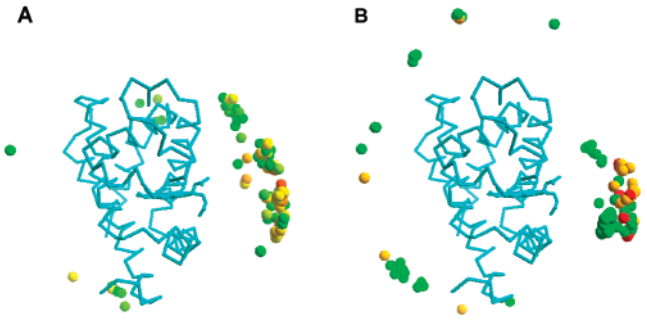

FIGURE 6: Comparison of the ab initio docking (A) and the docking with 15 NMR constraints (B), using BiGGER (*38*) for horse heart met-Mb and cyt b_5. The Mb is represented as a C^{α} trace (blue) and cyt b_5 as its center of mass for the top 100 docked geometries. The coloring of the spheres ranges from green to yellow to red and represents the scoring of the docked geometries from low to high.

overall correlation time (τ_r). The τ_r of free cyt b_5 and in the 1:1 complex with met-Mb was estimated according to eq 2. From a trimmed average $*T_1/T_2$ ratio excluding those values that differed by more than 10% from the mean, $\tau_r = 6.7$ ns for free cyt b_5 and 8.6 ns in a 1:1 mixture with met-Mb. From the titration curves, it is apparent that not all cyt b_5 is bound at a 1:1 stoichiometry, but approximately 74%. Due to the fast exchange regime on the NMR time scale, the T_1 and T_2 times are thus an average between the bound and free cyt b_5. The average T_1 and T_2 in the bound form are estimated with eq 3

$$T_{i\mathrm{obs}}^{-1} = f_b T_{ib}^{-1} + f_f T_{if}^{-1} \quad (3)$$

where i equals 1 or 2, T_{obs} is the observed relaxation rate, T_{ib} and T_{if} are the relaxation rates for bound and free cyt b_5, respectively, and f_b and f_f are the fractions of bound (0.74) and free (0.26) cyt b_5, respectively, yielding T_{1b} and T_{2b} values of 0.70 and 0.071 s, respectively. This gives a ratio, T_1/T_2, of 9.9, with an estimate for τ_r of 9.2 ns for fully bound cyt b_5, an increase of 73% compared to that for free cyt b_5.

Protein Docking. To visualize the binding site(s) on both proteins, protein docking simulations were performed with the program BiGGER (*38*). As no crystal structure of bovine Mb is known, the coordinates for horse Mb (*53*) were used instead. For the docking of Mb and cyt b_5, 5000 putative geometries generated by the program were independently assessed and ranked in terms of either the ab initio scoring function or the experimentally obtained data. The results of each ranking procedure are presented in Figure 6.

Using the ab initio approach (Figure 6A), the docked geometries for cyt b_5 form a broad hemisphere around the exposed heme edge of Mb. Using the 15 experimental constraints for cyt b_5 obtained from the NMR data, a slightly different picture of ranked docking geometries emerges (Figure 6B). Now, a more localized region of docked geometries is formed around the Mb heme, along with a number of additional docking sites scattered around the Mb. Of the 15 NMR constraints that were used, on average, four were violated. In both the ab initio and experimental approaches, the top-ranked solution is oriented at the exposed heme edge of the Mb, with the front face (acidic patches) of cyt b_5 and the heme 6-propionate involved in the binding interface. Fe−Fe distances of 13.3 and 11.6 Å for ab initio and experimental approaches, respectively, were obtained from the top-ranked solutions.

From the NMR titration experiments, it was noted that residues at the rear (in the N- and C-terminal regions) of cyt b_5 experienced a $\Delta\delta_{binding}$ (Figure 4). Analysis of the top 100 docking geometries using both the ab initio and NMR filter approaches revealed approximately 25% of the docked geometries were oriented in such a way that the N- and C-terminal regions of cyt b_5 were in close contact with Mb. This was true for docked geometries at the front face of Mb and for other Mb regions, further highlighting the possibility of numerous binding conformations for this complex.

DISCUSSION

Previous biochemical and biophysical studies (*17*, *23*, *33*, *34*) of the complex formed between Mb and cyt b_5 show that this particular complex is highly dynamic. Results of the current study using a combination of NMR chemical shift mapping, ^{15}N relaxation analysis, and protein docking simulations support the view that this complex exists in a dynamic ensemble of structures.

The dynamic nature is first apparent from the small size of the $\Delta\delta_{binding}$, with many of the affected residues being acidic in nature. A comparison can be drawn from the NMR study of the transient physiological complex between yeast cytochrome *c* peroxidase and ^{15}N-labeled cytochrome *c* (*10*). In this study, the effects are much larger with the maximum $\Delta\delta_{avg}$ for an amide of cytochrome *c* being 0.308 ppm. This is some 16 times larger (0.019 ppm for D82) than observed here for cyt b_5 (Figure 7). Furthermore, the largest $\Delta\delta_{avg}$ of perturbed cytochrome *c* resonances (0.101 ppm for T12, 0.308 ppm for Q16, 0.075 ppm for V28, and 0.110 ppm for F82) consist of hydrophobic and uncharged polar residues (*10*), buried in the complex interface according to the complex crystal structure (*65*). These findings suggested that cytochrome *c* occupied a single orientation for a significant fraction of the complex lifetime in solution, with water being stripped from the interface, allowing for hydrophobic interactions to anchor the complex in a single orientation (*10*). In contrast, for the cyt b_5−Mb complex, the acidic residues and the 6-propionate group of the heme appear to steer the cyt b_5 toward the Mb and sample a number of electrostatic orientations on the Mb surface. In these orientations, the residues in the interface may not be completely desolvated and at least a single layer of water molecules may remain. Furthermore, the chemical shift perturbations are averaged over all orientations. In combination, these effects may be the reason for the small chemical shift perturbations observed in the cyt b_5−Mb complex.

With a K_a ranging between 5(3) and 20(5) mM^{-1}, the interaction between bovine Mb and cyt b_5 is weak. This is in contrast to a previous 1D ^1H NMR study of a complex between bovine heart met-Mb and bovine liver cyt b_5 where a much stronger interaction for a 1:1 complex was obtained (K_a > 100 mM^{-1}, 30 mM sodium phosphate, pH 5.6, 298 K) (*32*). In the work presented here, the K_a values are closer to those previously reported for horse heart and sperm whale Mb upon interaction with bovine liver cyt b_5. For horse, values of 0.75 (ZnMb) and 1 mM^{-1} (met-Mb) have been determined (10 mM potassium phosphate, pH 6.0, 293 K) (*34*), while for sperm whale, a K_a of 3 mM^{-1} (ZnMb) is reported (10 mM potassium phosphate, pH 6.0, 293 K) (*33*). The magnitude of K_a values appears to be unrelated to

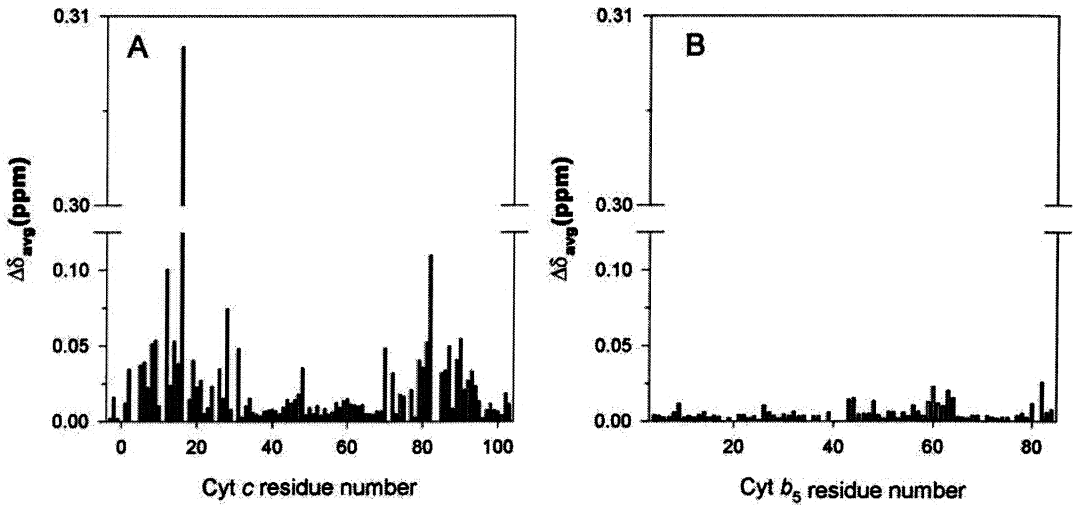

FIGURE 7: Comparison of the changes in average amide chemical shifts ($\Delta\delta_{avg}$) for (A) yeast cytochrome *c* upon interacting with cytochrome *c* peroxidase (>95% bound) (*10*) and (B) cyt b_5 upon interacting with met-Mb (extrapolated from Figure 3 to 100% bound) drawn to the same scale. Note the difference in $\Delta\delta_{avg}$ between a single orientation transient complex (A) and a dynamic ensemble of structures (B).

whether a transient complex exists in a single orientation or in a dynamic ensemble. For example, the complex of cytochrome *c* and plastocyanin has a K_a of 10^5 M^{-1} (similar to that of the cytochrome *c* peroxidase−cytochrome *c* complex) yet was suggested to exist in a dynamic ensemble of structures, dominated by electrostatics (*5*). This is further illustrated by the studies with cytochrome *f* and plastocyanin from plant and cyanobacterial sources. For these complexes, the K_a ranges between 10^2 M^{-1} (cyanobacterial)[2] and 10^4 M^{-1} (plant) at low ionic strengths. In both cases, a single orientation was observed, and intermolecular pseudocontact shifts could be detected (*6*, *11*). While the plant complex depends on both charged and hydrophobic interactions (*6*), the cyanobacterial complex is predominantly hydrophobic (*11*).

^{15}N relaxation data were obtained for cyt b_5 in the free state and in a mixture with Mb. From previous ^{15}N relaxation studies on bovine and rat cyt b_5 species, τ_rs ranging between 4.6 and 5.0 ns have been reported (*63*, *66*). We note here that our τ_r for the free protein of 6.7 ns is relatively high. This may be ascribed to the high protein concentration used for the measurements causing a more viscous sample and thus a longer correlation time. Aggregation is also possible at high concentrations, but no increase in line width was observed on comparing it with less concentrated samples of cyt b_5. From the Stokes−Einstein equation, an estimated 3-fold increase in τ_r for complex formation is predicted (*67*). The experimental value obtained here for τ_r of 9.2 ns for the bound form is therefore on the low side. However, it should be noted that the Stokes−Einstein relationship approximates the isotropic rotational correlation time for spherical molecules. Thus, the shape of the complex may play a role in determining the τ_r. Alternatively, the low τ_r for the complex could arise as a consequence of its highly dynamic nature, which would indicate that cyt b_5 possesses partial rotational freedom within the complex on the nanosecond time scale.

The NMR data indicate which residues of cyt b_5 are involved in complex formation. Clearly, the dominant interaction site includes the heme 6-propionate and acidic residues on the front face of cyt b_5. However, from Figures 3 and 4, it is evident that significant amide chemical shifts are also observed elsewhere on cyt b_5. In certain cases, the effects of binding a partner can be transmitted via H-bond networks to residues away from the binding site (*5*, *10*). In this case, the amides located toward the rear of cyt b_5 (in particular, L9, H80, and D82) are too far away, and are not involved in H-bond networks with the affected residues at the front, to arise from secondary shifts. The shifts at the back side most likely arise due to an alternative binding orientation and are thus in agreement with a multiconfiguration, dynamic docking model of the complex (*23*). Qualitatively, the binding maps for cyt b_5 are the same for complex formation with either redox state of Mb, although it is noted that Arg84 is affected by titration only with met-Mb, and Ala54 is affected by titration only with MbCO. However, the chemical shift changes in these two cases are small (Figure 3), and the differences may thus be insignificant. Also, the difference in K_a between met-Mb and MbCO is small, suggesting that the redox state of Mb has little effect on the dynamic ensemble. With this study being limited to the ferric form of cyt b_5, the possibility of the ferrous form yielding differences in complex formation cannot be ruled out.

From the protein docking program BiGGER (*38*), a picture of possible binding sites on Mb has been obtained. The picture from the ab initio approach is consistent with Brownian dynamic simulations (*17*, *33*, *34*) where a broad hemisphere of docked geometries is located around the exposed Mb heme. Interestingly, when NMR constraints are used, the docked geometries are more tightly clustered around the heme area on the Mb. This could indicate that the NMR data represent a certain subset of the possible docking configurations. The location of the dominant interaction site is in agreement with a recent ^{15}N,^{1}H-HSQC study of Mb reconstituted with heme propionamide (^{15}N) which showed that cyt b_5 interacts with the heme edge of Mb (*23*). The docking study also predicts that other satisfied docked geometries on the Mb surface exist (Figure 6B). Consistent with the dynamic docking model (*23*) and kinetics studies

[2] P. B. Crowley, unpublished results.

(*17*), the cyt b_5 appears to bind to a large area of the Mb surface in a wide variety of docked conformations, of which only a small subset of conformations around the heme of Mb can be ET-active. This is further emphasized from a recent cross-linking study of the cyt b_5−Mb complex, where it was found that cross-linking resulted in the entrapment of various protein orientations presumably formed in the encounter of the two proteins (*68*).

In conclusion, the results of this study further highlight the dynamic nature of the complex formed between Mb and cyt b_5. Characteristic features of the complex observed with NMR comprise the very small size of the chemical shift perturbations, the extensive surface area affected by complex formation, and the dominance of charged rather than hydrophobic and polar residues for the perturbed resonances. Future NMR studies on transient complexes may demonstrate whether these features can serve as general tools in distinguishing between a complex consisting of a single orientation and one that exists in a dynamic ensemble of orientations.

ACKNOWLEDGMENT

J.A.R.W. is indebted to Dr. M. C. Machczynski and Prof. G. W. Canters for many useful discussions.

SUPPORTING INFORMATION AVAILABLE

Two tables listing significant amide chemical shift changes for ferric cyt b_5 upon interaction with met-Mb and MbCO and ^{15}N relaxation times for cyt b_5 free and in a 1:1 stoichiometry with met-Mb. This material is available free of charge via the Internet at http://pubs.acs.org.

REFERENCES

1. McLendon, G. (1991) *Struct. Bonding 75*, 159−174.
2. Bendall, D. S. (1996) in *Protein Electron Transfer* (Bendall, D. S., Ed.) pp 43−68, BIOS Scientific Publishers, Oxford, U.K.
3. Yi, Q., Erman, J. E., and Satterlee, J. D. (1994) *Biochemistry 33*, 12032−12041.
4. Guiles, R. D., Sarma, S., DiGate, R. J., Banville, D., Basus, V. J., Kuntz, I. D., and Waskell, L. (1996) *Nat. Struct. Biol. 3*, 333−339.
5. Ubbink, M., and Bendall, D. S. (1997) *Biochemistry 36*, 6326−6335.
6. Ubbink, M., Ejdeback, M., Karlsson, B. G., and Bendall, D. S. (1998) *Structure 6*, 323−335.
7. Ejdebäck, M., Bergkvist, A., Karlsson, B. G., and Ubbink, M. (2000) *Biochemistry 39*, 5022−5027.
8. Morelli, X., Dolla, A., Czjzek, M., Nuno Palma, P., Blasco, F., Krippahl, L., Moura, J. J. G., and Guerlesquin, F. (2000) *Biochemistry 39*, 2530−2537.
9. Hom, K., Ma, Q.-F., Wolfe, G., Zhang, H., Storch, E. M., Daggett, V., Basus, V. J., and Waskell, L. (2000) *Biochemistry 39*, 14025−14039.
10. Worrall, J. A. R., Kolczak, U., Canters, G. W., and Ubbink, M. (2001) *Biochemistry 40*, 7069−7076.
11. Crowley, P. B., Otting, G., Schlarb-Ridley, B. G., Canters, G. W., and Ubbink, M. (2001) *J. Am. Chem. Soc. 123*, 10444−10453.
12. Hall, D. A., Vander Kooi, C. W., Stasik, C. N., Stevens, S. Y., Zuiderweg, E. R. P., and Matthews, R. G. (2001) *Proc. Natl. Acad. Sci. U.S.A. 98*, 9521−9526.
13. Bergvist, A., Ejdebäck, M., Ubbink, M., and Karlsson, B. G. (2001) *Protein Sci. 10*, 2623−2626.
14. Crowley, P. B., Rabe, K., Worrall, J. A. R., Canters, G. W., and Ubbink, M. (2002) *ChemBioChem 3*, 526−533.
15. Nocek, J. M., Zhou, J. S., DeForest, S., Priyadarshy, S., Beratan, D. N., Onuchic, J. N., and Hoffman, B. M. (1996) *Chem. Rev. 96*, 2459−2489.
16. Naito, N., Huang, H., Sturgess, W., Nocek, J. M., and Hoffman, B. M. (1998) *J. Am. Chem. Soc. 120*, 11256−11262.
17. Liang, Z.-X., Nocek, J. M., Kurnikov, I. V., Beratan, D. N., and Hoffman, B. M. (2000) *J. Am. Chem. Soc. 122*, 3552−3553.
18. Pletneva, E. V., Fulton, D. B., Kohzuma, T., and Kostic, N. M. (2000) *J. Am. Chem. Soc. 122*, 1034−1046.
19. Willie, A., Stayton, P. S., Sligar, S. G., Durham, B., and Millet, F. (1992) *Biochemistry 31*, 7237−7242.
20. Schlarb-Ridley, B. G., Bendall, D. S., and Howe C. J. (2002) *Biochemistry 41*, 3279−3285.
21. Hervas, M., Navarro, J. A., Molina-Heredia, F. P., and de la Rosa, M. A. (1998) *Photosynth. Res. 57*, 93−100.
22. Leesch, V. W., Bujons, J., Mauk, A. G., and Hoffman, B. M. (2000) *Biochemistry 39*, 10132−10139.
23. Liang, Z.-X., Nocek, J., Huang, K., Hayes, R. T., Kurnikov, I. V., Beratan, D. N., and Hoffman, B. M. (2002) *J. Am. Chem. Soc. 124*, 6849−6859.
24. Naito, A., Hui, H. L., Noble, R. W., and Hoffman, B. M. (2001) *Biochemistry 40*, 2060−2065.
25. Vergéres, G., and Waskell, L. (1995) *Biochimie 77*, 604−620.
26. Strittmatter, P., and Velick, S. (1956) *J. Biol. Chem. 221*, 253−264.
27. Fukushima, K., and Sato, R. (1973) *J. Biol. Chem. 74*, 161−173.
28. Oshino, N. (1978) *Pharmacol. Ther. 2*, 477−515.
29. Canova-Davis, E., and Waskell, L. (1984) *J. Biol. Chem. 259*, 2541−2546.
30. Wu, J., Gan, J.-H., Xia, Z.-X., Wang, H.-Y., Wang, W.-H., Xue, L.-L., Xie, Y., and Huang, Z.-X. (2000) *Proteins 40*, 249−257.
31. Hagler, L., Coppes, R. I., Jr., and Herman, R. H. (1979) *J. Biol. Chem. 197*, 87−104.
32. Livingston, D. J., McLachlan, S. J., LaMar, G. N., and Brown, W. D. (1985) *J. Biol. Chem. 260*, 15699−15707.
33. Nocek, J. M., Sishta, B. P., Cameron, J. C., Mauk, A. G., and Hoffman, B. M. (1997) *J. Am. Chem. Soc. 119*, 2146−2155.
34. Liang, Z.-X., Jiang, M., Ning, Q., and Hoffman, B. M. (2002) *J. Biol. Inorg. Chem. 7*, 580−588.
35. Funk, W. D., Lo, T. P., Mauk, M. R., Brayer, G. D., MacGillivray, R. T. A., and Mauk, A. G. (1990) *Biochemistry 29*, 5500−5508.
36. Zhu, Z., Cunane, L. M., Chen, Z.-W., Durley, R. C. E., Mathews, F. S., and Davidson, V. L. (1998) *Biochemistry 37*, 17128−17136.
37. Hippler, M., Drepper, F., Haehnel, W., and Rochaix, J.-D. (1998) *Proc. Natl. Acad. Sci. U.S.A. 95*, 7339−7344.
38. Palma, P. N., Krippahl, L., Wampler, J. E., and Moura, J. J. G. (2000) *Proteins 39*, 372−384.
39. Shimada, H., and Caughey, W. S. (1982) *J. Biol. Chem. 257*, 11893−11900.
40. Wittenberg, J. B., and Wittenberg, B. A. (1981) *Methods Enzymol. 76*, 29−42.
41. Reid, L. S., and Mauk, A. G. (1982) *J. Am. Chem. Soc. 104*, 841−845.
42. Ozols, J., and Strittmatter, P. (1964) *J. Biol. Chem. 239*, 1018−1023.
43. Anderson, P., Gsell, B., Wipf, B., Senn, H., and Otting, G. (1998) *J. Biomol. NMR 11*, 279−288.
44. Muskett, F. W., Kelly, G. P., and Whitford, D. (1996) *J. Mol. Biol. 258*, 172−189.
45. Kraulis, P. J. (1989) *J. Magn. Reson. 84*, 627−633.
46. Kraulis, P. J., Donaille, P. J., Campbell-Burk, S. L., van Aken, T., and Laue, E. D. (1994) *Biochemistry 33*, 3515−3531.
47. Garret, D. S., Seok, Y. J., Peterkofsky, A., Clore, G. M., and Gronenborn, A. M. (1997) *Biochemistry 36*, 4393−4398.
48. Kay, L. E., Nicholson, L. K., Delaglio, F., Bax, A., and Trochia, D. (1992) *J. Magn. Reson. 97*, 359−375.
49. Marquardt, D. W. (1963) *J. Soc. Ind. Appl. Math. 11*, 431−441.
50. Kay, L. E., Trochia, D. A., and Bax, A. (1989) *Biochemistry 28*, 8972−8979.
51. Lipari, G., and Szabo, A. (1982) *J. Am. Chem. Soc. 104*, 4546−4559.
52. Lipari, G., and Szabo, A. (1982) *J. Am. Chem. Soc. 104*, 4559−4570.
53. Evans, S. V., and Brayer, G. D. (1990) *J. Mol. Biol. 213*, 885−897.
54. Kurland, R. J., and McGarvey, B. R. (1970) *J. Magn. Reson. 2*, 286−301.
55. Bertini, I., and Luchinat, C. (1996) *Coord. Chem. Rev. 150*, 1−296.
56. LaMar, G. N., Budd, D. L., Viscio, D. B., Smith, K. M., and Langry, K. C. (1978) *Proc. Natl. Acad. Sci. U.S.A. 75*, 5755−5759.
57. Keller, R., and Wüthrich, K. (1980) *Biochim. Biophys. Acta 621*, 204−217.

58. LaMar, G. N., Burns, P. D., Jackson, J. T., Smith, K. M., Langry, K. C., and Strittmatter, P. (1981) *J. Biol. Chem. 256*, 6075−6079.
59. Nicholls, A., Sharp, K., and Honig, B. (1991) *Proteins 11*, 281−296.
60. Banci, L., Bertini, I., and Luchinat, C. (1994) *Methods Enzymol. 239*, 485−514.
61. Dangi, B., Blankman, J. I., Miller, C. J., Volkman, B. F., and Guiles, R. D. (1998) *J. Phys. Chem. B 102*, 8201−8208.
62. Assfalg, M., Banci, L., Bertini, I., Ciofi-Baffoni, S., and Barker, P. D. (2001) *Biochemistry 40*, 12761−12771.
63. Kelly, G. P., Muskett, F. W., and Whitford, D. (1997) *Eur. J. Biochem. 245*, 349−354.
64. Clore, G. M., Driscoll, P., Wingfield, P. T., and Gronenborn, A. M. (1990) *Biochemistry 29*, 7378−7401.
65. Pelletier, H., and Kraut, J. (1992) *Science 258*, 1748−1755.
66. Banci, L., Bertini, I., Cavazza, C., Felli, I. C., and Koulougliotis, D. (1998) *Biochemistry 37*, 12320−12330.
67. Cavanagh, J., Fairbrother, W. J., Palmer, A. G., III, and Skelton, N. J. (1996) *Protein NMR Spectroscopy Principles and Practice*, pp 1−24, Academic Press, San Diego.
68. Furukawa, Y., Matsuda, F., Ishimori, K., and Morishima, I. (2002) *J. Am. Chem. Soc. 124*, 4008−4019.

BI026296Y